GEOPHYSICS, VOL. 55, NO. 3 (MARCH 1990); P. 354–361, 8 FIGS., 2 TABLES.

Incorporation of topography into two-dimensional resistivity inversion

Lun-Tao Tong* and Chieh-Hou Yang*

ABSTRACT

Direct current resistivity data acquired on rough terrain can be interpreted by using an appropriate inversion technique after a topographic correction. In order to avoid the influence of a possibly incomplete topographic correction, an improved two-dimensional resistivity inversion algorithm has been developed to estimate the subsurface resistivity distribution in the presence of topography.

In this paper, fully discretized modeling is based on the finite-element method, and the iterative inversion scheme is derived from the second-order Marquardt damped least-squares method. The algorithm has been tested on both synthetic and field resistivity data with topography incorporated explicitly into the inversion model. Both theoretical and field studies indicate that the technique is computationally efficient and provides an improved geologic interpretation for complex subsurface structures. A four-electrode configuration is used in the algorithm so that the inversion can represent most field measurements.

INTRODUCTION

The interpretation of direct current (dc) resistivity data on a traverse across a buried two-dimensional (2-D) geoelectric structure is often analyzed by trial-and-error modeling. However, trial-and-error modeling requires a lot of interpreter interaction and gives little quantitative information about model resolution. Thus, a practical 2-D inversion technique for interpreting 2-D resistivity data is desired.

dc resistivity inversion has been investigated extensively. Pelton et al. (1978) developed an inexpensive computer algorithm for estimating the location and resistivity of a single 2-D prism with a rectangular cross-section. However, their algorithm cannot fit realistically complex models. Oristaglio and Worthington (1980) and Tripp et al. (1984) developed 2-D inversion algorithms for the line-source electromagnetic method and the dc resistivity sounding method, respectively. Although their sources were different, [the former used a 2-D source while the latter used a three-dimensional (3-D) source], their inversion schemes were quite similar and suitable for most complex 2-D models. Our inversion strategy is similar to theirs. We first divide the subsurface into several blocks and then estimate the resistivity of each block.

In the field, resistivity surveys sometimes are carried out in mountainous areas, where topographic effects may produce virtual anomalies in the resistivity section. Fox et al. (1980) showed a terrain-correction procedure to reduce the topographic effect in resistivity data, and Holcombe and Jiracek (1984) suggested that the corrected data could be interpreted as if they were the response of a flat-earth model. The resistivity response is affected not only by the structure of the irregular ground surface but also by the structure of the subsurface; the relationship between them is quite complicated. Hence, the resistivity anomalies due to topography may not be separated completely from those due to subsurface structures by using a simple correction for some complex 2-D geoelectric models. Furthermore, the addition of an artificial correction to the field resistivity data may contaminate the response of the subsurface geoelectrical structure.

To overcome the problem described above, we developed an algorithm for 2-D resistivity inversion in which topography is incorporated in the model. The finite-element mesh is defined in line with the electrode configuration and irregular ground surface. The subsurface is divided into several blocks whose resistivities are to be estimated. Thus, the resistivity data obtained from a rough terrain can be directly inverted to a subsurface resistivity distribution without applying any artificial corrections in advance.

There are three main differences between the approach described in this paper and that suggested by Tripp et al. (1984): first, we use a finite-element method while Tripp et

Manuscript received by the Editor January 4, 1988; revised manuscript received July 24, 1989.
*Energy and Resources Laboratories, Industrial Technology Research Institute, Chutung, Taiwan 31015, Republic of China.
‡Institute of Geophysics, National Central University, Chung-li, Taiwan 32054, Republic of China.

al. employ a transmission surface analogy for modeling; second, we explicitly incorporate the irregular surface instead of assuming a flat earth in the inversion scheme; and third, we use the four-electrode configuration instead of the dipole-dipole array only. The proposed inversion technique was applied to synthetic data and to field data from a fault zone and a river terrace in the Quaternary gravel-covered area in Taiwan. Our results demonstrate that the algorithm performs efficiently and produces reliable estimates of the subsurface resistivity.

MODELING TECHNIQUE

There are three main numerical techniques for modeling dc resistivity responses: the finite-difference, finite-element, and network analog methods. Since both the finite-difference and network methods use rectangular grids, which do not readily fit topography, we employ the finite-element method of Coggon (1971) and Rijo (1977). It is easy and efficient to describe the anomalous body and terrain surface using the finite-element mesh. Herein, we present only the basic equations.

Consider a 2-D geoelectric model with a point source on its surface. The basic concept of the finite-element solution scheme is to divide the region of interest into elements, and then to seek a solution in terms of the electric potential at the nodes of the mesh. The electric field induced by a point source is 3-D; it is necessary to remove its variation in the strike direction by Fourier transformation. Thus, in the transform domain, we can establish the following matrix equation:

$$\underline{\mathbf{K}}\boldsymbol{\Phi} = \mathbf{S}, \tag{1}$$

where $\underline{\mathbf{K}}$ is an L by L symmetric, sparse, banded, and tridiagonally dominant matrix, which is known as the stiffness matrix. The elements of this matrix depend upon the conductivities of the model and the values of the transform variables. L is the total number of nodes in the mesh. The vector $\boldsymbol{\Phi}$ comprises the unknown value of electric potential at each node in the transform domain. The vector $\mathbf{S}$ contains the current strength and position of the point source.

The electric potential at each node in the transform domain for a range of transform variables can be evaluated by the modified Cholesky method. We obtain the nodal potential in the space domain by inverse Fourier transformation using the technique suggested by Dey and Morrison (1979). Then, we can calculate the theoretical apparent resistivity response for any four-electrode configuration. The finite-element mesh was tested using 87 nodes in the horizontal direction and 17 nodes in the vertical direction. This mesh arrangement provides an acceptable accuracy of 4 percent in the apparent resistivity calculation for both Schlumberger and dipole-dipole arrays over a 100 $\Omega \cdot$ m half-space.

INVERSION METHOD

The application of the inversion technique to geoelectrical methods has been described before (e.g., Inman, 1975; Vozoff and Jupp, 1975). The Jupp-Vozoff algorithm, which is an iterative second-order Marquardt damped least-squares scheme, is used here. We present only the basic equations as they apply to the dc resistivity problem.

We assume that the N unknown model parameters $\mathbf{x}$ are related to the M resistivity data $\mathbf{d}$ by a nonlinear functional h defined as

$$\mathbf{d} = h(\mathbf{x}, c) \tag{2}$$

where c denotes the electrode separation. This nonlinear equation is linearized by expansion in a Taylor's series at each electrode separation. Elimination of the higher order terms leads to a linear set of M equations in N unknowns,

$$\boldsymbol{\Delta}\mathbf{d} = \underline{\mathbf{a}}\,\boldsymbol{\Delta}\mathbf{x}, \tag{3}$$

where

$$\Delta d_i = h(\mathbf{x}, c_i) - h(\mathbf{x}_0, c_i); \qquad i = 1, M, \tag{4}$$

$$a_{ij} = \partial h(\mathbf{x}, c_i)/\partial x_j\,|_{\mathbf{x}=\mathbf{x}_0}; \qquad i = 1, M; j = 1, N, \tag{5}$$

and

$$\boldsymbol{\Delta}\mathbf{x} = \mathbf{x} - \mathbf{x}_0. \tag{6}$$

The vector $\boldsymbol{\Delta}\mathbf{d}$ is the difference between the measured apparent resistivity data and the theoretical apparent resistivity of the initial model. The vector $\boldsymbol{\Delta}\mathbf{x}$ is the difference between the unknown model parameters and the initial model parameters. In our case, the model parameter is the resistivity of each block. The matrix $\underline{\mathbf{a}}$, sometimes known as the Jacobian matrix, is the matrix of partial derivatives of the apparent resistivities with respect to the model parameters.

Because both the model parameters and the resistivity data values may vary over several orders of magnitude, and also because they must be constrained to positive values, we use logarithmic fitting. Thus, let $\mathbf{D} = \ln \mathbf{d}$, $\mathbf{H} = \ln \mathbf{h}$, and $\mathbf{X} = \ln \mathbf{x}$. Using these equations and adding a data weighting matrix $\underline{\mathbf{W}}$ into the Jacobian matrix and equation (3),

$$A_{ij} = W_{ii}^{1/2}(\partial H_i/\partial X_j) \tag{7}$$

and

$$\boldsymbol{\Delta}\mathbf{D} = \underline{\mathbf{W}}^{1/2}(\mathbf{D} - \mathbf{H}) = \underline{\mathbf{A}}\,\boldsymbol{\Delta}\mathbf{X}. \tag{8}$$

The inverse procedure is to find the model parameters which minimize $\boldsymbol{\Delta}\mathbf{D}$. Since equation (8) was deduced by linearizing a nonlinear system, the solution requires several iterations. At each step, equation (8) is solved for $\boldsymbol{\Delta}\mathbf{X}$ and yields a new set of model parameters. This procedure is repeated until an accepted minimum-square residual is reached.

Gloub and Reinsch (1970) decomposed the Jacobian matrix $\underline{\mathbf{A}}$ into its row and column eigenvectors, and the associated singular values, as

$$\underline{\mathbf{A}} = \underline{\mathbf{U}}\underline{\boldsymbol{\Lambda}}\underline{\mathbf{V}}^T, \tag{9}$$

where $\underline{\mathbf{U}}$ is an M by M data eigenvector matrix, $\underline{\mathbf{V}}$ is an N by N solution eigenvector matrix, and $\underline{\boldsymbol{\Lambda}}$ is an N by N diagonal singular value matrix.

The parameter improvement vector $\boldsymbol{\Delta}\mathbf{X}$ is obtained by substituting $\underline{\mathbf{A}}$ from equation (9) into equation (8). The solution is

$$\Delta \mathbf{X} = \underline{\mathbf{V}}\underline{\Lambda}^{-1}\underline{\mathbf{U}}^T\Delta \mathbf{D}. \tag{10}$$

The problem is that when small singular values are present, the estimate for $\Delta \mathbf{X}$ is grossly contaminated by numerical noise. To overcome this problem, a damped N by N diagonal matrix $\underline{T}$ is added to equation (10); thus,

$$\Delta \mathbf{X} = \underline{\mathbf{V}}\underline{T}\underline{\Lambda}^{-1}\underline{\mathbf{U}}^T\Delta \mathbf{D}. \tag{11}$$

The elements of $\underline{\mathbf{T}}$ are

$$t_j = k_j^4/(k_j^4 + \mu^4), \tag{12}$$

where μ is known as the relative singular value threshold and $k_j = \lambda_j/\lambda_1$. λ_j is the jth singular value and λ_1 is the maximum of the singular values. The estimate is further stabilized by initially including only the largest singular values in the estimate. As the fitting error decreases, the singular values of less importance are also included in the estimate by initially giving μ a high value of 0.2 and then as the fitting error decreases, permitting μ to be decreased from iteration to iteration until it reaches a minimum allowed value.

Iterations are continued until an absolute (or relative) calculated error is within the desired bounds. After having found a model which fits the observed data, we calculate the root-mean-square (rms) relative error and the parameter covariance matrix (PCM). PCM is used to estimate how well the model parameters are fit. The rms and PCM values are given by

$$\text{rms} = \left[\frac{1}{M}\sum_{i=1}^{M}(H_i - D_i)^2/D_i^2\right]^{1/2} \tag{13}$$

and

$$\text{PCM} = \chi_\nu^2(\underline{\mathbf{A}}^T\underline{\mathbf{A}})^{-1}, \tag{14}$$

where χ_ν is known as the reduced chi-square defined by

$$\chi_\nu^2 = (\Delta \mathbf{D}^T\Delta \mathbf{D})/(M - N). \tag{15}$$

The square root of the diagonal elements of PCM gives us an estimate of the standard deviation of the predicted logarithmic parameter for each block resistivity.

In the above description, there is no implicit restriction on the choice of inversion model parameters. The model parameters may include resistivity and/or geometric parameters. In our application, the resistivity parameter is the resistivity of each block. The geometry of each block is specified and the topography is included explicitly. We estimate the resistivity of each block in the inversion process. The result is then the resistivity distribution under the specified irregular surface. The program developed for this application, implemented on an HP 900A, incorporated the following limits: the total number of permissible blocks is 54, defined on a finite-element mesh containing 169 and 17 nodes in the horizontal and vertical directions, respectively. 113 observed resistivity points are allowed.

CALCULATION OF THE JACOBIAN MATRIX

Part of the inversion process is evaluating the partial derivatives of the apparent resistivity with respect to the model parameters. Assume that ϕ_{i1} and ϕ_{i2} are the electric potentials for the potential electrodes labeled "1" and "2," respectively, at the ith measurement in the space domain. The measured apparent resistivity can be expressed as

$$\rho_{ai} = \frac{G_i}{I_i}|\phi_{i1} - \phi_{i2}|, \tag{16}$$

where ρ_a, G, and I are the apparent resistivity, geometric factor, and current strength, respectively. Thus, the partial derivative of ρ_a with respect to the model parameter x_j is given by

$$\frac{\partial \rho_{ai}}{\partial x_j} = \frac{G_i}{I_i}\left|\frac{\partial \phi_{i1}}{\partial x_j} - \frac{\partial \phi_{i2}}{\partial x_j}\right|. \tag{17}$$

Since ϕ is the inverse Fourier transform of Φ,

$$\frac{\partial \phi}{\partial x_j} = F^{-1}\left(\frac{\partial \Phi}{\partial x_j}\right). \tag{18}$$

where F^{-1} denotes the inverse Fourier transform. Thus, the evaluation of the partial derivative of Φ with respect to x_j is the key point in the calculation of the Jacobian matrix. We differentiate the matrix equation (1) with respect to the jth model parameter with the assumption that the source is independent of the model parameter. The result is

$$\underline{\mathbf{K}}\frac{\partial \mathbf{\Phi}}{\partial x_j} = -\frac{\partial \underline{\mathbf{K}}}{\partial x_j}\mathbf{\Phi}. \tag{19}$$

Since $\underline{\mathbf{K}}$ is the sum of simple element matrices, its derivative with respect to x_j can be assembled from the appropriate derivatives of the element matrices. Thus the derivative of $\mathbf{\Phi}$ with respect to parameter x_j can be obtained by solving equation (19). Apart from the finite-element approximation, equation (19) is an exact analytical equation for the partial derivatives, so the partial derivatives can be calculated as accurately as the electric potential. The partial derivative of the apparent resistivity with respect to the model parameter for a four-electrode arrangement can be computed easily by combining equations (17), (18), and (19).

THEORETICAL TESTING AND VERIFICATION

Numerical tests on both noise-free and noisy 2-D synthetic resistivity data measured along an irregular surface have been undertaken to evaluate the capabilities and limitations of our inversion algorithm. The synthetic data are the computed apparent resistivities for a Schlumberger array or a dipole-dipole array on a traverse perpendicular to the strike of the 2-D earth model. For the models shown in Figure 1, the earth surface has a slope between electrodes labeled "0" and "1." Two models, a fault (model 1) and a river terrace (model 2), are considered. Because it is difficult to distinguish these structures based on topography only, our purpose is to demonstrate the utility of our inversion algorithm in distinguishing the two structures and to examine the adaptability of the topographic correction.

A conventional topographic correction (Fox et al., 1980) was employed to modify the synthetic dipole-dipole resistivity data from model 1. Figure 2a shows the final corrected resistivity pseudosection of this model, while Figure 2b shows the computed resistivity pseudosection of a similar

model with no topography. A comparison between Figure 2a and Figure 2b reveals substantial differences. Furthermore, the determination of an appropriate reference datum for the topographic correction is difficult. Thus, the conventional topographic correction seems inadequate in this case. Explicitly including the topography into the model avoids the problem altogether, thereby allowing us to invert to a more accurate subsurface resistivity structure directly. Since the resolution of the resistivity structure becomes worse with increasing depth, we divide the shallow structure into smaller blocks and the deep structure into large blocks.

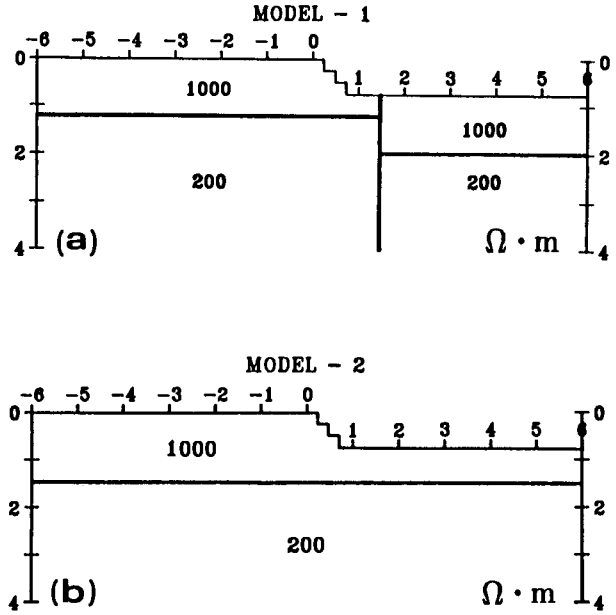

FIG. 1. The surface slope models used for the synthetic data: (a) fault model, (b) river terrace model.

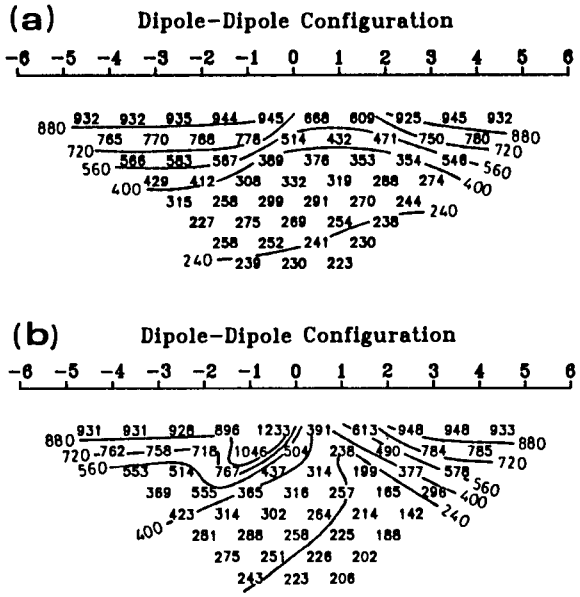

FIG. 2. (a) Conventional topography-corrected resistivity pseudosection of the results of fault model of Figure 1a for dipole-dipole array. (b) The synthetic dipole-dipole resistivity pseudosection of a flat surface fault model having the same throw as the fault model shown in Figure 1a. Contour intervals on pseudosection are 160 Ω · m.

To determine whether the inversion method could successfully locate the boundaries and the resistivity of each block in the presence of topography, we set the resistivity of the starting model for all blocks at 500 Ω · m. Figure 3 shows the 2-D discretized inversion of the data from the models in Figure 1. The block resistivities of the inverted models, whose response fit the synthetic noise-free data of model 1 and model 2 to acceptable values, are shown in Table 1. This inversion routine requires three to ten iterations to converge to the final model. Although the resistivity of each block is different from the true resistivity, one can easily discriminate the subsurface structure from the obvious resistivity contrasts. For example, from the inversion results of model 1 in Table 1, there is a 7:1 resistivity contrast between block numbers 2 and 3. The same result can be noted between block numbers 23 and 24, which defines the bottom of the upper layer very well. Although the contrast between block numbers 11 and 15 shows a lack of resolution of the features on both sides, the character of the fault structure is still obvious.

Figure 4 gives the standard deviations of the predicted logarithmic parameters for each block; these are predictions of the confidence intervals for the variations of the resistivities of the blocks on a logarithmic scale. Figure 4 shows that the confidence intervals for the lower blocks are large, while those for the upper blocks are small. The standard deviation is affected by the size and the position of the block. Blocks which are small in size or are far from the observing point contribute less to the measured resistivity data. Parameters for those blocks are ill-determined. To overcome this problem, small blocks with approximately the same resistivity are combined into large blocks, increasing the convergence rate and decreasing the total number of inversion parameters.

To test the effect of noise on the inversion, 10 percent

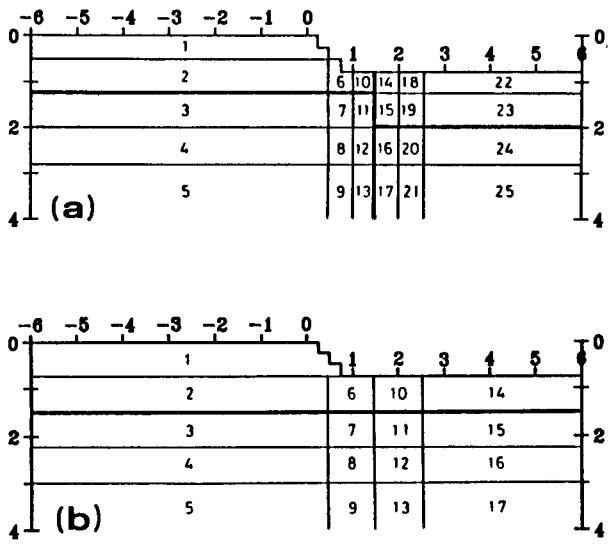

FIG. 3. Structures of the models used for inverting the (a) fault model and (b) river terrace model. The blocks for each model are outlined.

random Gaussian noise was added to the synthetic data of model 1 and model 2. The initial models are the same as those used previously. Table 2 lists the inversion results for noisy data from model 1 and model 2. The subsurface structures delineated by these inversions are still obvious.

The preceding experiments show that our inversion program is able to resolve complex 2-D models for noise-free and noisy resistivity data for different electrode arrangements in the presence of topography.

INVERSION OF FIELD DATA

To demonstrate the ability of our inversion algorithm to interpret actual 2-D resistivity data measured along a rough surface, two sites located at a gravel-covered area in the Hou-li tableland of west-central Taiwan were chosen. These sites are similar to the synthetic models: test site 1 is a fault structure and test site 2 is a river terrace.

Owing to a lack of information from outcrops and wells in the survey areas, we used one-dimensional (1-D) inversion results of vertical electric sounding (VES) data with Schlumberger arrays to construct the initial model for the 2-D inversion. Each Schlumberger array has a direction which is roughly parallel to the strike of the earth structure.

The accuracy of the forward solution for different electrode configurations and different terrains is important. Therefore, one must design an optimum finite-element mesh before inverting the data. Based on our inversion studies with synthetic and field data, we suggest the following inversion procedures:

(1) Collect geologic data, geophysical data, and related information from outcrops, wells, and former studies in the neighborhood of the traverse.
(2) Design a finite-element mesh for the electrode configuration used in the field work.
(3) Based on the information from outcrops, wells, and the 1-D inverse results from VES, divide the subsurface into several blocks as a preliminary model.
(4) Convert the apparent resistivity pseudosection into a geoelectric section by using the 2-D inversion algorithm.
(5) Interpret the final model.

Test site 1

Fifteen Schlumberger VES stations were selected. The spread of the current electrode ranged from 380 to 500 m, and the traverse was perpendicular to the Tachia-tung fault. There is a 2.5 m elevation change between locations with x-coordinates of -15 and -20 units in Figure 5. In order to fit the 2-D assumption, the electrode spread at each station along this traverse was perpendicular to the fault strike; while the electrode spreads of the stations off the traverse were parallel to the fault strike. The inversion results from these data were stitched together and used for the initial model for the 2-D inversion. Figure 5 shows the field resistivity pseudosection.

The finite-element mesh used had 169 nodes in the horizontal direction and 18 nodes in the vertical direction. The subsurface was divided into 54 blocks as shown in Figure 6a. Figure 6b shows the final geoelectrical model with 3.33 percent rms relative error after seven iterations. The upper layer with higher resistivity corresponds to the lateritic gravel of the tableland, while the lower resistivity layer under the gravel bed corresponds to the sand-clay stone of the Toukoshan formation. The lateritic gravel bed in Figure 6b has an inclined and discontinuous shape and has almost the same resistivity value on both sides of the fault. Furthermore, the gravel beds on both sides of the fault belong to the same lithologic age; and the inclined stratum was formed prior to faulting. Thus, the fault structure is obviously delineated.

Test site 2

Seven Schlumberger stations and a dipole-dipole traverse with a dipole length of 40 m were acquired at this site. There is an elevation change of nearly 10 m between locations with x-coordinates of -6 and 2 units in Figure 7, which also shows the measured apparent-resistivity pseudosection for this traverse. The subsurface was divided into 31 blocks, as

Table 1. The resistivity of each block from the inversion of model 1 and model 2 synthetic Schlumberger and dipole-dipole array responses (noise-free).

BLOCK NUMBER		1	2	3	4	5	6	7	8	9	10
MODEL-1	SCH	940	1118	97.4	334	282	643	435	222	153	810
	D-D	936	1093	148	173	185	823	136	279	293	746
MODEL-2	SCH	993	1032	170	184	244	1008	235	109	273	1009
	D-D	969	1092	141	142	265	883	386	262	318	1008
BLOCK NUMBER		11	12	13	14	15	16	17	18	19	20
MODEL-1	SCH	157	152	134	897	709	266	149	854	1583	213
	D-D	512	259	305	1117	673	292	313	1120	589	276
MODEL-2	SCH	162	313	330	1009	184	275	139			
	D-D	149	194	328	1064	175	177	281			
BLOCK NUMBER		21	22	23	24	25					
MODEL-1	SCH	165	991	1016	260	135					
	D-D	324	982	1040	155	251					

shown in Figure 8a. In this case, the finite-element mesh used had 87 by 22 nodes in the horizontal and vertical directions, respectively. Figure 8b is the final model with a 4.89 percent rms relative error after six iterations.

The upper layer with higher resistivity again corresponds to the lateritic gravel of the tableland, while the lower resistivity layer beneath corresponds to the sand-clay stone of the Toukoshan formation. As shown in Figure 8b, the upper layer of the gravel bed has different resistivity values (approximately 450 $\Omega \cdot$ m in the northern section and 650 $\Omega \cdot$ m in southern section) on both sides of the slope. The lower layer has the same resistivity value (about 180 $\Omega \cdot$ m) on both sides. Although there are some higher resistivity zones in the northern part of the interpreted geoelectric section, this may be the result of measurement errors or noise in the resistivity data. The different resistivity values of the upper gravel layer on the two sides of the slope indicate that the two gravel units belong to different depositional units, while the lower layer units with the same resistivity values evidently belong to the same depositional unit. Thus, the structure of the river terrace is clearly delineated.

We conclude from these field studies that our 2-D inversion algorithm allows direct interpretation of the resistivity data measured on a rough surface.

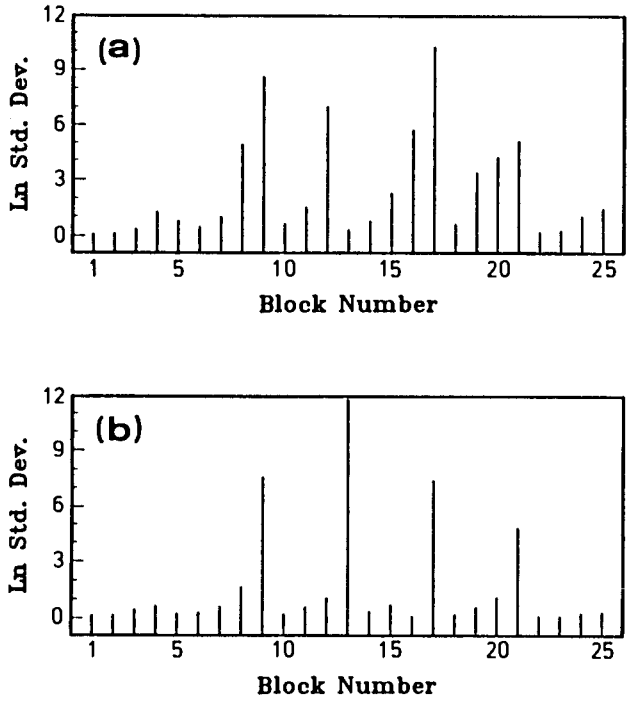

FIG. 4. The predicted standard deviation of the logarithmic parameter based on the inversion results for the fault model (noise-free case) for (a) Schlumberger array and (b) dipole-dipole array.

CONCLUSIONS

We have presented an inversion algorithm which can be used for the automatic 2-D interpretation of resistivity data measured on irregular topography. We incorporate topography into the inversion model explicitly. Therefore, the measured resistivity data can be inverted directly to determine the subsurface structure. The results of both theoretical and field studies show that this inversion algorithm provides a rapid and efficient analysis of the resistivity data. Our algorithm can deal with any four-electrode configuration. Any available information related to the subsurface structure in a study area can be used to construct the initial model. A presurvey study of inverting the resistivity data based on initial-guess models for different electrode configurations may allow the designing of a more efficient electrode configuration for detecting presumed subsurface structures.

The limitations of this 2-D inversion technique are the following: (1) The geometry of the subsurface must be specified in advance. (2) The total number of inversion parameters allowed may be limited. (3) The process of dividing the subsurface into blocks must be done carefully, because a smaller block will lead to a poorer resolution of the resistivity and an increase in the number of iterations. (4) The surface elevation and the distance between electrodes

Table 2. The resistivity of each block from the inversion of model 1 and model 2 synthetic Schlumberger and dipole-dipole array response (10% random noise added).

BLOCK NUMBER		1	2	3	4	5	6	7	8	9	10
MODEL-1	SCH	805	1172	150	65.7	698	715	625	345	34.3	1584
	D-D	915	978	224	150	161	1063	118	304	313	1044
MODEL-2	SCH	926	1074	158	128	376	1031	169	178	651	693
	D-D	907	1126	149	117	317	904	257	340	327	971
BLOCK NUMBER		11	12	13	14	15	16	17	18	19	20
MODEL-1	SCH	98.8	216	76.1	511	542	178	82.0	908	2299	81.7
	D-D	266	392	328	1699	792	365	346	1345	357	479
MODEL-2	SCH	265	189	255	911	322	136	115			
	D-D	128	416	332	1129	144	150	365			
BLOCK NUMBER		21	22	23	24	25					
MODEL-1	SCH	100	990	933	590	109					
	D-D	362	1548	750	207	324					

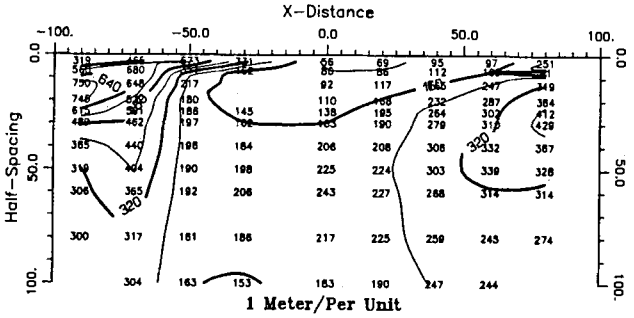

FIG. 5. The apparent resistivity pseudosection of traverse AA′ at test site 1 of the Hou-li tableland. Contour interval on pseudosection is 80 Ω · m.

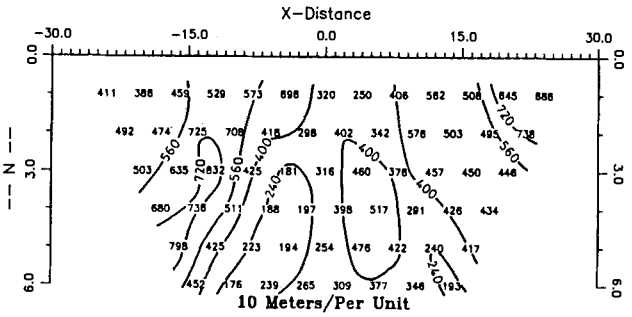

FIG. 7. The apparent resistivity pseudosection of traverse BB′ at test site 2 of the Hou-li tableland. Contour interval on pseudosection is 160 Ω · m.

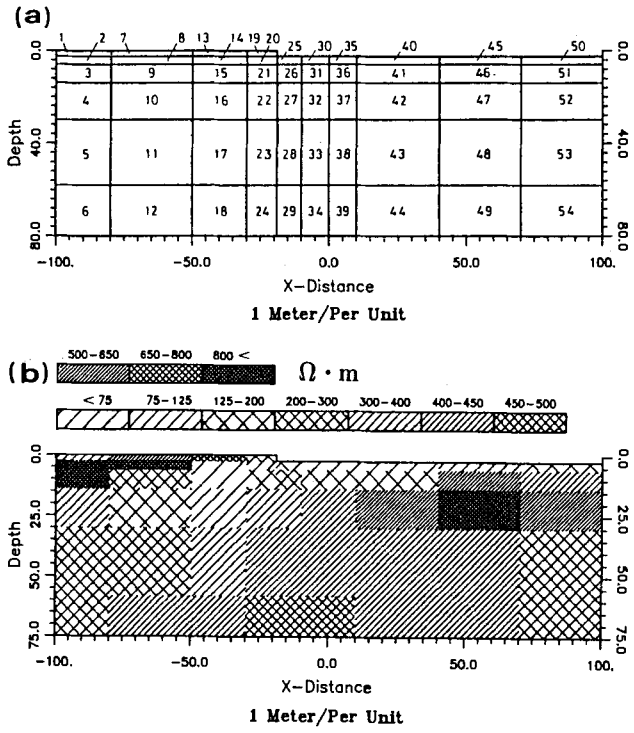

BLOCK NO	1	2	3	4	5	6	7	8	9	10	11	12	13
RESISTIVITY	377	1353	1534	380	222	286	534	835	288	168	216	405	690

BLOCK NO	14	15	16	17	18	19	20	21	22	23	24	25	26
RESISTIVITY	65.7	39.5	125	318	435	222	94.8	192	355	417	464	182	254

BLOCK NO	27	28	29	30	31	32	33	34	35	36	37	38	39
RESISTIVITY	346	436	471	48.5	191	416	440	468	54.8	195	423	446	470

BLOCK NO	40	41	42	43	44	45	46	47	48	49	50	51	52
RESISTIVITY	67.3	131	516	409	421	96.1	576	815	426	441	193	412	521

BLOCK NO	53	54
RESISTIVITY	233	255

FIG. 6. (a) The inversion model structure (54 blocks); (b) the final model with 3.33 percent rms relative error after seven iterations.

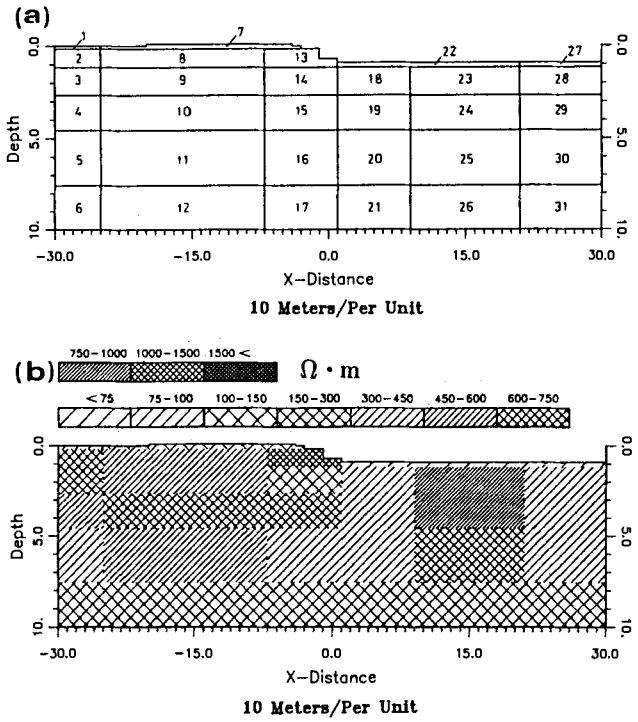

BLOCK NO	1	2	3	4	5	6	7	8	9	10	11	12	13
RESISTIVITY	96.7	713	667	564	310	193	133	596	557	695	482	274	1173

BLOCK NO	14	15	16	17	18	19	20	21	22	23	24	25	26
RESISTIVITY	237	601	354	180	352	431	388	168	40.4	814	761	632	232

BLOCK NO	27	28	29	30	31
RESISTIVITY	66.0	402	392	390	187

FIG. 8. (a) The inversion model structure (31 blocks); (b) the final model with 4.89 percent rms relative error after six iterations.

must be measured as accurately as possible; otherwise, the erroneous elevation and distance will result in a biased interpretation. The same problem exists in the traditional topographic correction procedure. (5) It is not possible to evaluate the effect of 3-D topography and subsurface structures from the 2-D inversion results. However, the use of the algorithm is practical, rapid, and reliable for delineating the subsurface structures within the limitations mentioned above. This methodology can be used to analyze 2-D resistivity data from surveys carried out on either a flat or irregular topographic surface.

REFERENCES

Coggon, J. H., 1971, Electromagnetic and electrical modeling by the finite-element method: Geophysics, **36**, 132–155.

Dey, A., and Morrison, H. F., 1979, Resistivity modeling for arbitrarily two-dimensional structures: Geophys. Prosp., **27**, 106–136.

Fox, R. C., Hohmann, G. W. Killpack, T. J., and Rijo, L., 1980, Topographic effects in resistivity and induced-polarization surveys: Geophysics, **45**, 75–93.

Golub, G. H., and Reinsch, C., 1970, Singular value decomposition and least-squares solutions: Num. Math., **14**, 403–420.

Holcombe, H. T., and Jiracek, G. R., 1984, Three-dimensional terrain corrections in resistivity surveys: Geophysics, **49**, 439–452.

Inman, J. R., 1975, Resistivity inversion with ridge regression: Geophysics, **40**, 798–817.

Jupp, D. L. B., and Vozoff, K., 1975, Stable iterative methods for geophysical inversion: Geophys. J. Roy. Astr. Soc., **42**, 957–976.

Oristaglio, M. L., and Worthington, M. H., 1980, Inversion of surface and borehole electromagnetic data for two-dimensional electrical conductivity models: Geophys. Prosp., **28**, 633–657.

Pelton, W. H., Rijo, L., and Swift, C. M., 1978, Inversion of two-dimensional resistivity and induced-polarization data: Geophysics, **43**, 788–803.

Rijo, L., 1977, Modeling of electric and electromagnetic data: Ph. D. thesis, Univ. of Utah.

Tripp, A. C., Hohmann, G. W., and Swift, C. M., 1984, Two-dimensional resistivity inversion: Geophysics, **49**, 1708–1717.

Vozoff, K., and Jupp, D. L. B., 1975, Joint inversion of geophysical data: Geophys. J. Roy. Astr. Soc., **42**, 977–991.